Histochemistry and Cell Biology
https://doi.org/10.1007/s00418-020-01855-z

ORIGINAL PAPER

Accurate and live peroxisome biogenesis evaluation achieved by lentiviral expression of a green fluorescent protein fused to a peroxisome targeting signal 1

Tanguy Demaret[1] · Guillaume E. Courtoy[2] · Joachim Ravau[1] · Patrick Van Der Smissen[3] · Mustapha Najimi[1] · Etienne M. Sokal[1]

Accepted: 17 February 2020
© Springer-Verlag GmbH Germany, part of Springer Nature 2020

Abstract

Peroxisomes are ubiquitous organelles formed by peroxisome biogenesis (PB). During PB, peroxisomal matrix proteins harboring a peroxisome targeting signal (PTS) are imported inside peroxisomes by peroxins, encoded by *PEX* genes. Genetic alterations in *PEX* genes lead to a spectrum of incurable diseases called Zellweger spectrum disorders (ZSD). In vitro drug screening is part of the quest for a cure in ZSD by restoring PB in ZSD cell models. In vitro PB evaluation is commonly achieved by immunofluorescent staining or transient peroxisome fluorescent reporter expression. Both techniques have several drawbacks (cost, time-consuming technique, etc.) which we overcame by developing a third-generation lentiviral transfer plasmid expressing an enhanced green fluorescent protein fused to PTS1 (eGFP–PTS1). By eGFP–PTS1 lentiviral transduction, we quantified PB and peroxisome motility in ZSD and control mouse and human fibroblasts. We confirmed the stable eGFP–PTS1 expression along cell passages. eGFP signal analysis distinguished ZSD from control eGFP–PTS1-transduced cells. Live eGFP–PTS1 transduced cells imaging quantified peroxisomes motility. In conclusion, we developed a lentiviral transfer plasmid allowing stable eGFP–PTS1 expression to study PB (deposited on Addgene: #133282). This tool meets the needs for in vitro PB evaluation and ZSD drug discovery.

Keywords Peroxisome biogenesis · Peroxisome biogenesis disorder · Zellweger spectrum disorder · Peroxisome targeting signal · Lentivirus

Introduction

Peroxisomes are single membrane-bound ubiquitous organelles involved in numerous metabolic pathways including very long- and branched-chain fatty acids oxidation, and reactive oxygen species detoxification (Wanders 2014). They are formed and maintained in a process called peroxisome biogenesis (PB) [reviewed in (Fujiki 2016)]. PB is governed by proteins called peroxins (PEX) through processes including peroxisome membrane assembly, peroxisomal matrix protein import, and peroxisome fission. Peroxisomal matrix protein import begins by the recognition of a peroxisome targeting signal (PTS) 1 or 2 (by PEX5 or PEX7, respectively) on matrix proteins newly synthetized in the cytosol [reviewed in (Dias et al. 2016; Emmanouilidis et al. 2016)]; afterwards, the matrix proteins are translocated into the peroxisome lumen, and finally, PEX5 and PEX7 are released in the cytosol for another round of import. Along with PB, peroxisome proliferation, peroxisome autophagy (i.e.,

Electronic supplementary material The online version of this article (https://doi.org/10.1007/s00418-020-01855-z) contains supplementary material, which is available to authorized users.

✉ Etienne M. Sokal
etienne.sokal@uclouvain.be

[1] Laboratoire d'Hépatologie Pédiatrique et Thérapie Cellulaire, Unité PEDI, Institut de Recherche Expérimentale et Clinique (IREC), Université Catholique de Louvain (UCLouvain), 1200 Brussels, Belgium

[2] IREC Imaging Platform (2IP), Institut de Recherche Expérimentale et Clinique (IREC), Université Catholique de Louvain (UCLouvain), 1200 Brussels, Belgium

[3] Platform for Imaging Cells and Tissues (PICT), de Duve Institute, Université Catholique de Louvain (UCLouvain), 1200 Brussels, Belgium

Published online: 02 March 2020

pexophagy), and peroxisome motility take part in the peroxisome homeostasis in response to external stimuli [reviewed in (Neuhaus et al. 2016)]. Beside their complex biogenesis and regulation, peroxisomes are in close contact with other organelles like mitochondria and the endoplasmic reticulum [reviewed in (Farre et al. 2019)].

Genetic alterations in *PEX* genes lead to peroxisome biogenesis disorder (PBD) in cells and Zellweger spectrum disorders (ZSD) in patients [reviewed in (Argyriou et al. 2016)]. ZSD is a continuum spectrum between severely affected patients (former Zellweger syndrome) which die of a progressive liver insufficiency during the first year of life, to mildly affected patients (former infantile Refsum disease) which suffer from leukodystrophy, failure to thrive, developmental delay, and hepatic dysfunction. These patients rarely survive after the third decade and the lack of independent living skills is the most handicapping (Berendse et al. 2016). To date, supportive management is considered the standard of care, as no validated curative treatment has shown clinical benefits (Klouwer et al. 2015). In the quest for a cure, liver and hepatocyte transplantation (Demaret et al. 2018; Matsunami et al. 2016; Sokal et al. 2003; Van Maldergem et al. 2005) have been used to deliver a large amount of functional peroxisomes to patients, with clinical and biological success. Beside this cellular approach, a molecular approach based on in vitro drug screening aims at restoring PB in cell models before starting clinical trials. Several compounds (arginine, betaine, hydroxychloroquine, etc.) are able to restore PB in vitro, mostly in cell carrying the *PEX1-G843D* hypomorphic mutation (Berendse et al. 2013; Law et al. 2017; MacLean et al. 2019; Wei et al. 2000; Zhang et al. 2010). This molecular approach requires powerful tools to evaluate PB in vitro, especially in cell donors harboring peroxisomal mosaicism. Peroxisomal mosaicism refers to heterogeneous peroxisome labeling in cell population (see below) in which some cells harbor import-competent peroxisomes, while adjacent cells contain import-deficient peroxisomes (ghosts) (Argyriou et al. 2016). Peroxisomal mosaicism was reported in fibroblasts and liver biopsies from mild ZSD patients (Giros et al. 1996; Mandel et al. 1994).

Immunofluorescence (IF) and transient peroxisomal fluorescent reporter transfection are two techniques of choice to evaluate PB in vitro. IF labeling a peroxisomal membrane protein [e.g., the 70-kDa peroxisomal membrane protein (PMP70)] and a peroxisomal matrix protein (e.g., the catalase) allows import-competent peroxisomes identification by measuring colocalization between both markers (Soliman et al. 2018). Colocalization is lower in ZSD cells than in control, because the catalase is not properly imported inside peroxisomes (PMP70-positive particles). Plasmid transfection is a second approach used to transiently express a fluorescent protein fused to a PTS which drives the reporter to peroxisomes (Koster and Waterham 2017). This technique demonstrates a diffuse cytosolic signal or a punctiform pattern in ZSD and control cells, respectively (Ebberink et al. 2011; Sexton et al. 2010). IF and transient peroxisomal fluorescent reporter transfection have several drawbacks such as the heaviness and the cost of the techniques. Moreover, the fixation required by IF precludes any dynamic study and the transfection technique is hampered by its cell toxicity, its transientness, and a low efficiency, especially on primary cells such as human fibroblasts (Schrader et al. 2017).

To overcome all these limitations, we developed a third-generation lentiviral transfer plasmid expressing an enhanced green fluorescent protein (eGFP) fused to a PTS1 (eGFP–PTS1). By this approach, we obtained a highly efficient and stable eGFP–PTS1 expression both in mouse and human fibroblasts. eGFP automated signal analysis allowed to distinguish efficiently ZSD from control cell donors and to quantify peroxisome motility.

Materials and methods

Cell isolation and culture

Control and ZSD human fibroblasts were obtained by skin biopsy from a previously reported patient with *PEX1* deficiency, after written informed consent (Demaret et al. 2018; Sokal et al. 2003). Mouse fibroblasts from $Pex1^{wt/wt}$ and $Pex1^{G844D/G844D}$ embryos were collected from a mild ZSD mouse model as described previously (Hiebler et al. 2014; Tymms and Kola 2001). We selected the *Pex1-G844D* mouse model, because the mutation is equivalent to the common *PEX1–G843D* hypomorphic human mutation. The *Pex1–G844D* mutation confers a high level of peroxisomal mosaicism in ZSD fibroblasts. It challenged our method to distinguish between control and ZSD cell donors (Berendse et al. 2019). Mice experiments were approved by the Ethical Committee for Animal Experimentation at the Health Science Sector, UCLouvain, Brussels, Belgium (2017/UCL/MD/006). Both cell types were cultured in Dulbecco's Modified Eagle Medium high glucose (DMEM, Gibco, 41965-039) supplemented with 10% fetal bovine serum (FBS, Gibco, 10270-106) and 1% penicillin/streptomycin (P/S, Gibco, 15140-122), and cultured at 37 °C in a fully humidified atmosphere containing 5% CO_2. Cells were trypsinized (Trypsin–EDTA, Gibco, 25300-054) and seeded at a defined frequency and density (Table 1). Cell viability was always > 95% as measured by trypan blue 0.2% exclusion assay (HyClone, Thermo Fisher Scientific, SV30084.01).

Peroxisome targeting signal cloning

The eGFP fused to PTS1 from pEGFP-C1 + SKL (Addgene #53450) was amplified by polymerase chain reaction (PCR)

Table 1 Characteristics of the fibroblasts analyzed and transduced

Species	Age	Disease status	Plating density	Passage	Passages during the study
Mouse	E13.5[a]	Control	15,000 cells/cm^2	Twice a week	P4–P27
Mouse	E13.5[a]	ZSD	15,000 cells/cm^2	Twice a week	P5–P42
Human	9 years	Control	5000 cells/cm^2	At 80% confluency	P3–P17
Human	18 years	ZSD	5000 cells/cm^2	At 80% confluency	P8–P22

[a]Mouse embryonic day

(GoTaq G2 Hot Start Polymerase, Promega, M740A) according to the manufacturer's instructions. Primer sequences were F-5′-GGCACCAAAATCAACGGGAC-3′ and R-5′-GGCGGTCGACGTTTCAGGTTCAGGGGGAGG-3′ (including a 5′ non-hybridizing SalI restriction site—underlined). The PCR product and pRRLSIN.cPPT.PGK-GFP.WPRE (Addgene #12252) were separately digested overnight (ON) at 37 °C with 10 U SalI (SalI, Thermo Fisher Scientific, #ER0641) and 10 U BsrGI (Bsp1407I, Thermo Fisher Scientific, #ER0931) in Tango 2X buffer (Tango Buffer 10X, Thermo Fisher Scientific, BY5) (Fig. 1a). Restriction enzyme heat inactivation at 65 °C for 20 min was performed on the digested products. A small amount of the digested products was run on a 1% agarose gel (UltraPure Agarose, Invitrogen, 15510-027) containing intercalating agent diluted 1/20.000 (Midori Green Advance DNA Stain, Nippon Genetics, MG04) at 120 V during 45 min to confirm the successful digestion. Ligation was performed with a 1:3 vector:insert molar ratio according to the manufacturer's instructions (T4 DNA Ligase, New England, BioLabs, M0202S). Chemically competent *E. coli* were transformed with the ligation product (One Shot TOP10, Thermo Fisher Scientific, C404006) and plated onto LB agar plate containing ampicillin 100 µg/mL (Ampicillin sodium salt, Gibco, 11593027). Colonies were screened by PCR with the following primers F-5′-GTGTTCCGCATTCTGCAAG-3′ and R-5′-AGCAGCGTATCCACATAGCG -3′. Ladder (GeneRuler 1 kb Plus DNA Ladder, Thermo Fisher Scientific, SM1334) and PCR products were run on a 1% agarose gel showing a 925 or 1067 bp product for the native and the modified vector, respectively (Fig. 1b). Plasmid amplification and purification (PureYield Plasmid Maxiprep System,

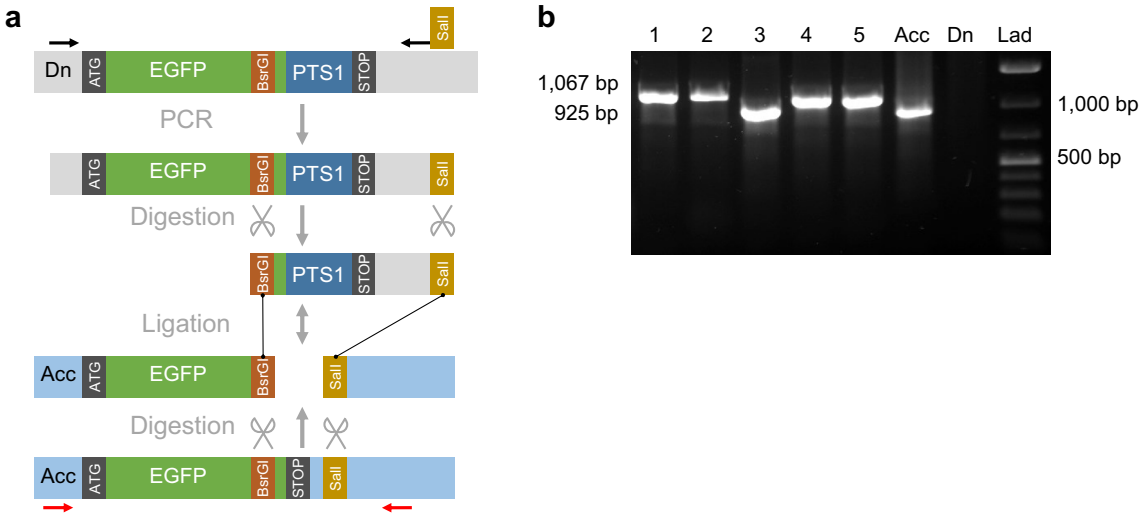

Fig. 1 **a** Cloning approach outline. The open reading frame of enhanced green fluorescent protein (EGFP) fused to the peroxisome targeting signal 1 (PTS1) was amplified from a donor plasmid (Dn). During amplification, a SalI restriction site was created thanks to a non-hybridizing 5′ end on the reverse primer (black arrow with box). The amplicon and the acceptor plasmid (Acc) were digested with BsrGI and SalI. Both digestion products were ligated and the ligation product was transformed in chemocompetent bacteria. Red arrows below the acceptor plasmid represents the primers used to run screening PCR on bacterial colonies emerging after transformation. **b** Agarose gel of the colony screening PCR products. Products from colonies (1–5) and controls (Acc and Dn) were run on gel electrophoresis. Colonies 1, 2, 4, and 5 PCR produced a 1067 base pairs (bp) fragment showing genetic material insertion between primers compared to the 925 bp fragment of the Acc PCR. Dn PCR amplified no fragment as the PCR was designed for. Colony 3 PCR amplified a 925 bp because of cloning failure

Promega, A2392) was performed on a colony containing the modified vector (pRRLSIN.cPPT.PGK-GFP-PTS1.WPRE). Next-generation sequencing confirmed the expected plasmid sequence (Online Resources 1–4). The amplified plasmid passed the quality controls from a nonprofit plasmid repository and is available in open access (Addgene, #133282).

Lentivirus production

HEK293FT cells (Invitrogen, R70007, cultivated according to the provider's instructions) at 70% confluency on CELLSTAR Cell Culture Flasks (Greiner Bio-One, 690 175) were transfected with PTS1 modified lentiviral transfer plasmid pRRLSIN.cPPT.PGK-GFP-PTS1.WPRE (Addgene, #133282), and pCMV-VSV-G, pMDLg/pRRE, pRSV-Rev (Addgene, #8454, #12251, #12253) third-generation lentiviral packaging system in a 4/1/1/1 molar ratio using Lipofectamine 2000 Transfection Reagent (Thermo Fisher Scientific, 11668-030) in Opti-MEM (Gibco, 31985-062) according to the manufacturer's instructions. After 6 h, transfection medium was replaced by growing medium without antibiotics. Every 24 h for 3 days, the eGFP–PTS1 lentivirus-containing supernatant (eGFP–PTS1–LV) was harvested, centrifuged for 5 min at 2500 *g* to remove cell debris, and aliquoted and stored at − 80 °C.

Fibroblasts ($n = 4$) at 50–70% confluency were incubated 48 h with eGFP–PTS1–LV and hexadimethrine bromide at a final concentration of 6 µg/mL (Sigma-Aldrich, H9268, diluted in distilled water and filtered at 0.22 µm). Transduced cells were expanded, trypsinized, and suspended at 10^7 cells/mL in 0.22 µm filtered phosphate-buffered saline (PBS, Lonza, 15-512F), 2% FBS, and 1 mM ethylenediaminetetraacetic acid tetrasodium salt hydrate (EDTA, Sigma-Aldrich, E5391-250G). Fluorescence-activated cell sorting (FACS) on an FACSAriaIII (BD Biosciences) was used to collect eGFP-positive (eGFP+) fibroblasts (i.e., eGFP–PTS1 transduced cells). To avoid the sorting of cell doublets or cell aggregates, single cells were sequentially selected on forward scatter area (FSC-A)/forward scatter width (FSC-W) and side scatter area (SSC-A)/side scatter width (SSC-W) dot plots. The sorting was performed using an 85 µm nozzle at 45 psi, and a flow rate that allowed collecting 2000 events per second. The data acquisition and analysis were performed using the FACSDiva software (BD Biosciences). The sorting was performed to get at least 150,000 eGFP+ cells, and purity was verified a first time just after the sorting and a second time > 5 passages after sorting.

Immunofluorescence

Fibroblasts seeded on 12 mm round autoclaved glass coverslips no. 1 (VWR, 631-1577) in 24-well plates (Greiner Bio-One, 662 160) were fixed with 1 volume formaldehyde 4% (VWR, 11699408) on culture medium (formaldehyde final concentration of 2%) during 5 min at room temperature (RT) and then 10 min with the original solution (formaldehyde final concentration of 4%). Fixed cells were washed three times with PBS and permeabilized with Triton-X100 0.5% (Sigma-Aldrich, X100-500ML) in PBS (PBS tablets diluted in distilled water, Gibco, 18912-014) during 15 min at RT. Permeabilized cells were washed three times with PBS and a blocking step was achieved with 1 h incubation in normal goat serum 5% (NGS, Sigma-Aldrich, G9023-10ML) in PBS at RT. Cells were incubated ON at 4 °C with primary antibodies anti-catalase (Thermo Fisher Scientific, A21987, lot 1673440) and anti-PMP70 (Abcam, ab85550, lot GR99621-1) diluted in NGS 0.5% in PBS at 1/100 and 1/1000, respectively. Cells were washed three times with PBS and incubated with AlexaFluor 488 goat anti-mouse (Thermo Fischer Scientific, A11001) and AlexaFluor 594 goat anti-rabbit (Thermo Fischer Scientific, A11012) diluted in NGS 0.5% in PBS at 1/500 for 90 min at RT and protected from light. Control immunolabeling was performed with secondary antibodies alone. Immunolabeled cells were washed three times with PBS and nuclei were stained with diamidino-2-phenylindole dihydrochloride (DAPI, Sigma-Aldrich, D9542-1MG) diluted in distilled water at a final concentration of 0.2 µg/mL. Cells were washed three times with PBS and they were mounted with fluorescence mounting medium (Dako, S3023) on Superfrost Plus slides (Thermo Fisher Scientific, J1800AMNT). Cells were imaged on a cell observer spinning disk confocal microscope (Zeiss) using a Plan Apochromat 100×/1.4 Oil DICII objective.

eGFP–PTS1 transduced cells seeded on µ-Slide glass bottom (Ibidi, 80287) were imaged at 37 °C during all the acquisition with a picture taken every 10 s for 45 cycles.

Image analysis

Our strategy was to detect PBD with a relatively small number of cell pictures. Overlap and correlation of catalase/eGFP–PTS1 and PMP70 signals were investigated by calculating Manders' overlap coefficient (MOC, measure of the fraction of overlapping pixels) and Pearson's correlation coefficient (PCC, measure of the covariance in the two signals) using Axiovision v. 4.8.2.0 (Zeiss). Using a fixed intensity threshold for each signal, we defined four zones on a scatter-plot. Zone 3 was the zone above the threshold for both signals. MOC and POC were calculated on zone 3 (Online Resource 5). Illustrative image profiles were obtained with ZEN 2.3 Blue Edition (Zeiss).

Peroxisomes automated quantification was performed with ImageJ 1.52p (National Institutes of Health). Native high-definition (.czi) images were imported using Bio-Formats 6.3. The green (eGFP) and the blue (DAPI) channels were sequentially analyzed with a macro. In the green

channel, the mean intensity of total image was measured for each sample. In a second step, the peroxisomes were segmented into individual particles according to the green signal. The number, size (μm^2), and mean intensity of the individualized peroxisomes were calculated using the AnalyzeParticles tool. Finally, nuclei were counted using the same approach in the blue channel for normalization purposes.

Time-lapse analysis

The image sequences (45 frames, one every 10 s) were opened in native high-definition format (.czi) with ImageJ 1.52p (National Institutes of Health). The signal was normalized by local contrast to ensure a homogeneous illumination throughout the sequence. The bright spots corresponding to the peroxisomes were then analyzed with the TrackMate plugin (Tinevez et al. 2017). As a result, the maximal speed for each individual track (referred to as peroxisome track maximal velocity) was calculated and exported for statistical analysis.

Figure drawing and statistical analysis

Publisher (Office 365, Microsoft) was used to draw the figures. Two-tailed Mann–Whitney tests or Student's *t* test with confidence intervals of 95% were performed using GraphPad Prism v.5.02 for Windows (GraphPad Software). *P*-values < 0.05 were considered significant.

Results

Peroxisome targeting signal 1 (PTS1) was functionally cloned in eGFP lentiviral vector allowing stable eGFP–PTS1 expression

Peroxisome targeting signal 1 (PTS1) was cloned in frame at the 3′ extremity of the eGFP in the third-generation lentiviral transfer plasmid (Fig. 1a). A screening PCR designed to encompass the cloning site in the acceptor plasmid showed an increased fragment length in accordance with the cloned fragment (Fig. 1b). HEK293FT cells transiently transfected with the original (pRRLSIN.cPPT.PGK-GFP.WPRE) or the PTS1 modified (pRRLSIN.cPPT.PGK-GFP-PTS1.WPRE) lentiviral transfer plasmids harbored a diffuse green signal (cytosolic location) or a punctiform green signal (peroxisomal location), respectively (Fig. 2a). This highlighted the modified eGFP localization achieved by PTS1 cloning.

Fibroblasts ($n = 4$) were transduced with eGFP–PTS1–LV. FACS on the four cell populations measured a transduction efficiency ranging from 44.4% (cryopreserved lentiviruses) to 86.5% (freshly produced lentiviruses) (Fig. 2b). After eGFP+ cell sorting, ~ 100% of the cells were eGFP+ and this was conserved in all donors after > 8 passages (Fig. 2c). All the eGFP–PTS1 analyses described below were carried out on the four donors sorted populations.

Decreased catalase + PMP70 colocalization confirmed PBD in ZSD cells

Double IF targeting a peroxisomal matrix protein (catalase) and a peroxisomal membrane protein (PMP70) was performed to evaluate PB in cells, as published previously (Santos et al. 1988).

Catalase staining distribution was punctiform in control donors but lighter and more diffuse (in mouse fibroblasts) in the cytoplasm of ZSD cells, suggesting a lack of peroxisomal catalase import (i.e. PBD) (Figs. 3a1–4). In ZSD mouse fibroblasts, some cells displayed clear punctiform catalase staining next to cells with diffuse catalase staining (peroxisomal mosaicism) (Fig. 3a2).

PMP70 staining evidenced a lower number of peroxisomes with enlarged size or irregular shape (peroxisomal ghosts) in ZSD donors than in controls (Fig. 3a5–8, see inserts). Size and number of peroxisomal ghosts were previously reported to depend on the *PEX* mutation (Soliman et al. 2018).

The low or absent catalase + PMP70 colocalization in ZSD donors confirmed the PBD. The distinct signal colocalizations in adjacent ZSD mouse fibroblasts brought firmly the peroxisomal mosaicism to light (Fig. 3a10).

Profile lines were drawn on merged images to precisely visualize the catalase + PMP70 colocalization (Fig. 3a13–16). The peroxisomal mosaicism in ZSD mouse fibroblasts was highlighted by the presence of colocalized green and red signal next to individual red or green peaks on the same profile line. MOC and PCC were calculated for catalase and PMP70 signals. MOC and PCC were higher in controls compared to ZSD donors (Fig. 3b, c). Furthermore, among ZSD donors, MOC and PCC were particularly low in ZSD human fibroblasts, demonstrating the very low colocalization and underlying the absence of peroxisomal mosaicism in this donor.

eGFP–PTS1 + PMP70 colocalization was efficient to evaluate PB

We measured eGFP–PTS1 + PMP70 colocalization to evaluate PB. We confirmed that eGFP–PTS1 + PMP70 colocalization was similar to catalase-PMP70 colocalization achieved by IF.

eGFP–PTS1 signal was punctiform in control fibroblasts and diffuse in ZSD fibroblasts cytoplasm (Fig. 4a1-4). In eGFP–PTS1 transduced ZSD mouse fibroblasts, peroxisomal

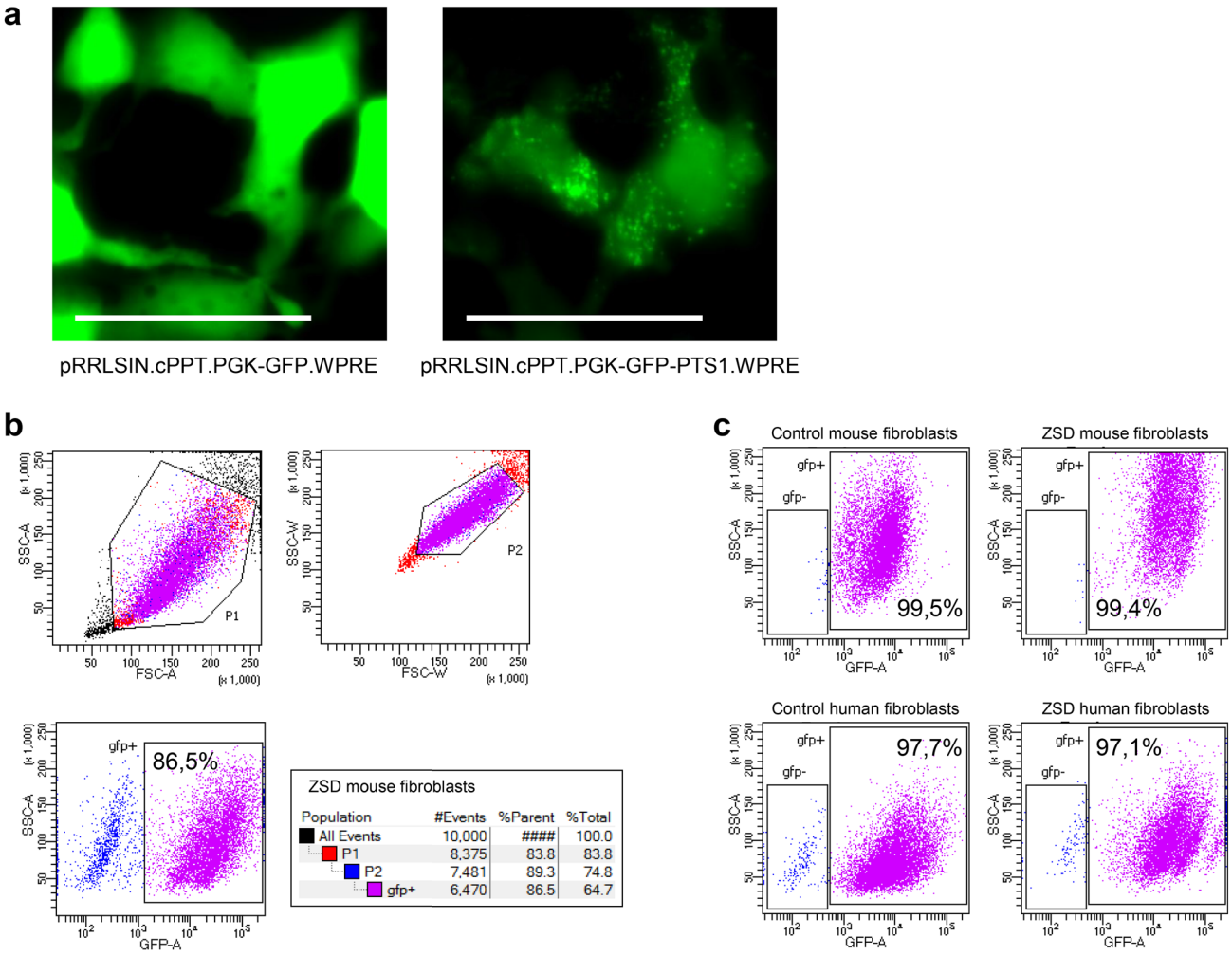

Fig. 2 **a** HEK293FT transfected with pRRLSIN.cPPT.PGK-GFP.WPRE (left panel) or pRRLSIN.cPPT.PGK-GFP-PTS1.WPRE (right panel). Note the change in enhanced green fluorescent protein (eGFP) localisation achieved by peroxisome targeting signal 1 (PTS1) cloning. Scale bar: 50 µm. **b** Cell sorting strategy after pRRLSIN.cPPT.PGK-GFP-PTS1.WPRE transduction. Before sorting, 86.5% of the ZSD mouse fibroblasts were eGFP-positive. **c** Side scatter area (SSC-A)/eGFP area dot plots correspond to the 4 transduced donors > 8 passages after cell sorting. The analysis showed eGFP signal stability (> 97%)

mosaicism was detected (Fig. 4a2) similar to what catalase IF demonstrated (Fig. 3a2).

Transduced cells were labeled by PMP70 IF. The low eGFP–PTS1 + PMP70 colocalization in ZSD donors confirmed the PBD (Fig. 4a10, 12). Profile lines were drawn on merged images to visualize the eGFP–PTS1 + PMP70 colocalization (Fig. 4a13–16). The different eGFP–PTS1 + PMP70 colocalization profiles in adjacent ZSD mouse fibroblasts confirmed peroxisomal mosaicism in this donor (Fig. 4a10). Peroxisomal mosaicism was further highlighted by the presence of colocalized green and red signals next to individual red or green peaks on the same profile line (Fig. 4a14).

MOC and PCC were calculated to quantify the correlation between eGFP–PTS1 and PMP70 signals. MOC and PCC were higher in control donors than in ZSD donors (Fig. 4b, c). Among ZSD donors, MOC and PCC were strongly reduced in ZSD human fibroblasts, underlying the absence of peroxisomal mosaicism in this donor.

These results demonstrated that PMP70 colocalized with our eGFP–PTS1 fusion product, and that eGFP–PTS1 + PMP70 signals was as sensitive as common IF protocol (catalase + PMP70) to evaluate PB in vitro.

eGFP–PTS1 signal alone allowed PB evaluation and peroxisome morphometry in living cells

eGFP signal from the 4 eGFP–PTS1 transduced donors was analyzed alone to evaluate PB without the need for cell transfection nor IF. Signal analysis was performed with ImageJ using the AnalyzeParticles tool (Fig. 5a).

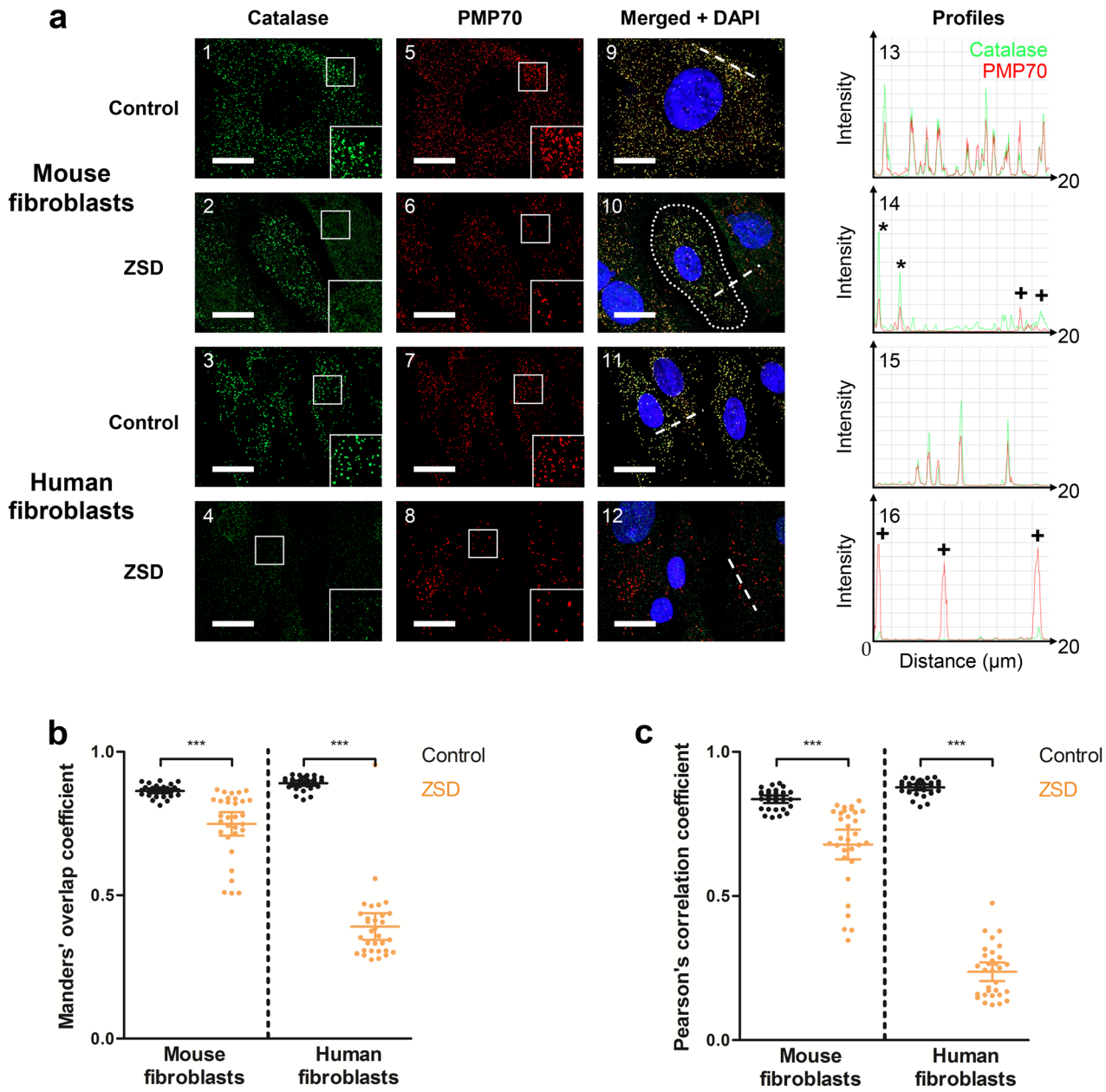

Fig. 3 **a** Catalase (green) and 70-kDa peroxisomal membrane protein (PMP70, red) immunofluorescence (IF) staining. Inserts show higher magnification of the boxed area. IF highlighted a lower colocalization of both signals in Zellweger spectrum disorder (ZSD) donors. Peroxisomal mosaicism (i.e., a mixed population of cells with and without functional peroxisome biogenesis) was detected in ZSD mouse fibroblasts as shown inside the dotted area (a10). Dotted lines localize the profile analysis (a13–16). In ZSD donors, profiles showed no localized correlation of intensities between both signals (marked with +), representing peroxisome biogenesis disorder. In ZSD mouse fibroblasts, some localized correlations of intensities were still present (marked with asterisk) representing residual peroxisome biogenesis among the peroxisome biogenesis disorder (i.e., peroxisomal mosaicism). Nuclei are stained with diamidino-2-phenylindole dihydrochloride (DAPI). Scale bar: 20 µm. Representative pictures of 30 micrographs by donor. **b** Manders' overlap coefficient (MOC) and **c** Pearson's correlation coefficient (PCC) graphs representing correlation of catalase and PMP70 signals among the four donors. MOC ranges from 0 to 1 and PCC ranges from −1 to 1, with higher values indicating stronger correlation. Both coefficients concluded to a lower correlation (i.e., colocalization) in ZSD donors than in controls. Unpaired Student's *t* test two-tailed, $n = 30$, mean ± 95% confidence interval, $***p < 0.0001$

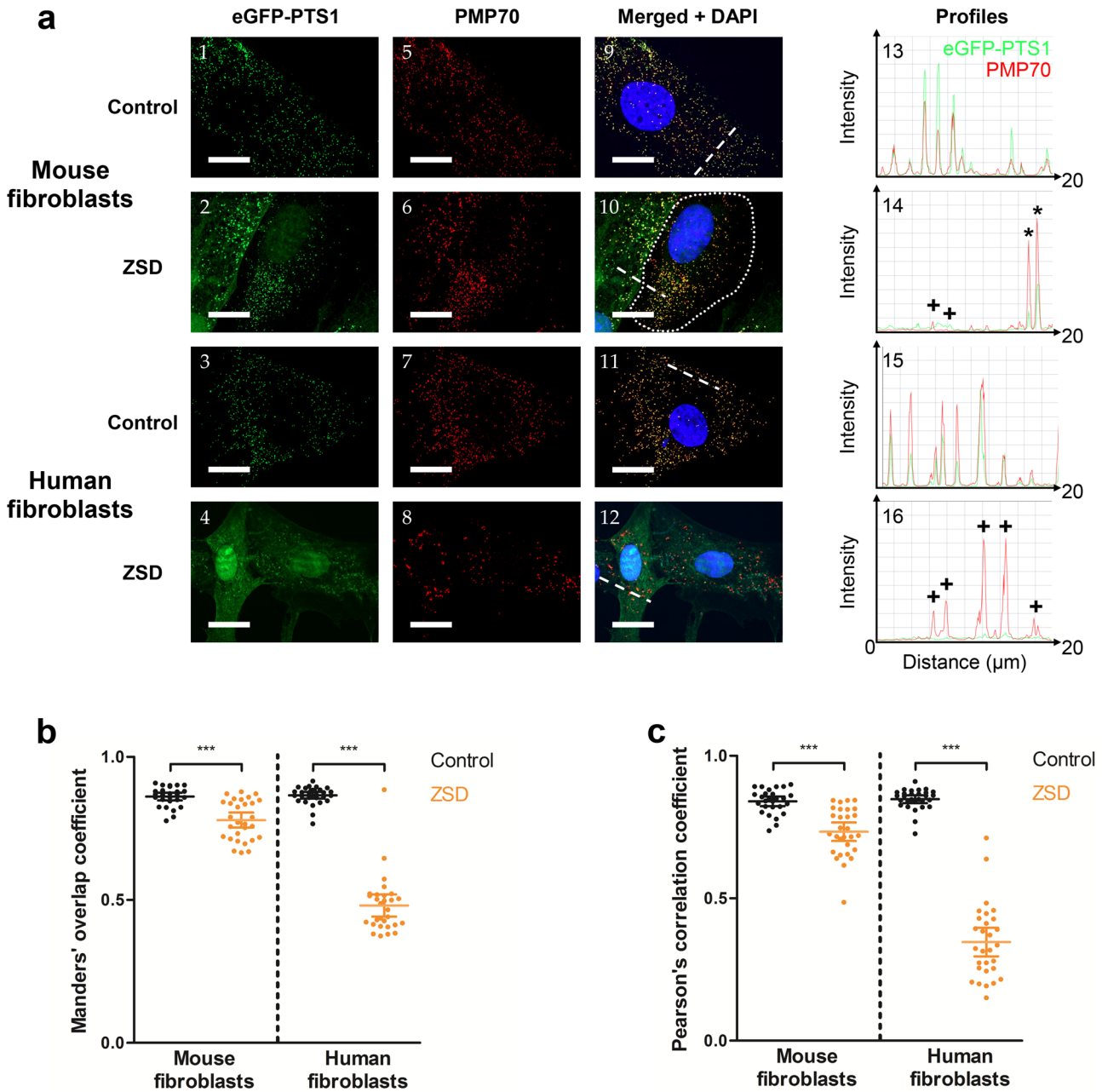

Fig. 4 **a** 70-kDa peroxisomal membrane protein (PMP70, red) immunofluorescent staining on cells transduced with an enhanced green fluorescent protein fused to a peroxisome targeting signal 1 (eGFP–PTS1). This method highlighted lower signal colocalization in Zellweger spectrum disorder (ZSD) donors. Peroxisomal mosaicism (i.e., a mixed population of cells with and without functional peroxisome biogenesis) was detected in ZSD mouse fibroblasts as shown inside the dotted area (a10). Dotted lines localize the profile analysis (a13–16). In ZSD donors, profiles showed the absence of localized correlation of intensities between both signals (marked with +), representing peroxisome biogenesis disorder. In ZSD mouse fibroblasts, some localized correlations of intensities were still present (marked with asterisk) representing residual peroxisome biogenesis among the peroxisome biogenesis disorder (i.e., peroxisomal mosaicism). Nuclei were stained with diamidino-2-phenylindole dihydrochloride (DAPI). Scale bar: 20 µm. Representative pictures of 30 micrographs by condition. **b** Manders' overlap coefficient (MOC) and **c** Pearson's correlation coefficient (PCC) graphs representing the colocalization of eGFP–PTS1 and PMP70 signals among the four donors. MOC ranges from 0 to 1 and PCC ranges from −1 to 1, with higher values indicating stronger colocalization. Both coefficients highlighted lower colocalization in ZSD donors. Unpaired Student's *t* test two-tailed, $n = 30$, mean ± 95% confidence interval, ***$p < 0.0001$

Among the four eGFP–PTS1 transduced donors, eGFP signal mean intensity (i.e., on the entire micrograph) was significantly higher in ZSD donors, indicative of a more diffuse eGFP signal in these donors (Fig. 5b). Concerning eGFP+ particles, the mean intensity was higher in controls than in ZSD donors, suggesting stronger eGFP–PTS1 peroxisomal import in control donors (Fig. 5b).

In human fibroblasts, the eGFP+ particles number (normalized per cell number) and the average size (in μm^2) of these particles were significantly lower in ZSD than in control fibroblasts (Fig. 5b). These results indicate that ZSD human fibroblasts contained less peroxisome matrices, of smaller size and with weaker eGFP signal than control cells.

Peroxisome motility was analyzed on photographs taken every 10 s from living cells transduced with eGFP–PTS1 (Online Resources 6, 7). The time-lapses were analyzed using automated tracking tool to quantify eGFP+ particles motility and peroxisome track maximal velocity (i.e., the maximal velocity recorded for each peroxisome) (Fig. 5c). In ZSD human fibroblasts, the fastest particles were significantly slower than in controls as shown by the cumulative incidence of the peroxisome track maximal velocity (Fig. 5d) and on the 25 fastest velocities recorded from the 4 donors (Fig. 5e).

Discussion

The aim of this study was to develop a new accessible method to evaluate PB in vitro. Our third-generation lentiviral vector allowed persistent expression of eGFP–PTS1 fusion product and stable fluorescent signal along cell passages in control and ZSD mouse and human fibroblasts. First, eGFP–PTS1 pattern was similar to catalase, a peroxisomal matrix protein. Second, eGFP–PST1 colocalization with PMP70, a peroxisome membrane protein, was similar to catalase colocalization with PMP70, demonstrating correct technical sensitivity and no eGFP–PTS1 fusion product interaction with PB. Third, eGFP–PTS1 signal alone was sufficient to discriminate ZSD from control cells and allowed live cell imaging for peroxisome motility quantification.

eGFP–PTS1–LV allowed us to reach up to > 85% transduction efficiency on primary cells. After eGFP+ cell sorting, the signal remained > 97% for more than eight passages without any sign of signal loss. Our FACS approach collected cells with different eGFP–PTS1 expression levels among the same population (Fig. 2c). This did not impede the precision of the different parameters measured afterwards. Yet, a more stringent cell sorting approach (i.e., a narrower positive cell gating) could potentially lead to reduced dispersion of the parameters measured.

Classical PB evaluation is achieved by transient transfection of a peroxisomal reporter plasmid with cationic lipid transfection agents such as Lipofectamine [36] or microporation [37]. Lipofectamine transfection efficiency is very low on primary cells (< 1% in our experience on skin fibroblasts) and the compound exhibits cell toxicity. Microporation is more efficient than Lipofectamine on primary cells, but requires tricky optimization steps and expensive single-use cassettes [20]. Both techniques lead to transient protein expression and thus require transfection step before every experiment. Moreover, PTS1 protein import pathway is saturable (Brickner et al. 1997). Since transient transfection achieve high protein expression levels (Hunter et al. 2019), PTS1 protein import pathway saturation by highly expressed eGFP–PTS1 thanks to transient transfection cannot be excluded. To our knowledge, the transfection or microporation effect on PB was never studied. After establishing transduced cells population, fibroblasts are ready for many experiments without potentially confounding factors.

Peroxisomes size and speed measured by eGFP–PTS1 particle analysis and tracking were comparable to previous publication based on eGFP–PTS1 transient transfection (Metz et al. 2017). The cloning steps did not impede the correct eGFP–PTS1 localization. The lentiviral transduction did not modify the peroxisome matrix microscopic characteristics.

eGFP–PTS1 signal and catalase IF staining colocalized with PMP70 IF staining depending on the cell PB capacity. MOC and PCC used to quantify this colocalization as the reflect of PB in our study were previously used to study pexophagy by the colocalization of catalase or PMP70 with autophagy receptors (Deosaran et al. 2013; Marcassa et al. 2018) and to decipher the link between peroxisomes and the endoplasmic reticulum (Mast et al. 2016). MOC quantifies the overlap between two signals without evaluating the intensity of them, whereas PCC takes the intensity into account to give a correlation coefficient. In our study, both MOC and PCC gave similar results, because green and red signal overlapped and were also positively correlated in intensity. Using these two methods, we demonstrate the colocalization of PMP70 with catalase and eGFP–PTS1 in peroxisomes of cells with functional PB and evidence the defective important in ZSD cells.

eGFP+ particles number, eGFP+ average area, and peroxisome track maximal velocity were statistically different between control and ZSD donors in human fibroblasts but not in mouse fibroblasts. This could be explained by peroxisomal mosaicism highlighted by eGFP–PTS1 signal in ZSD mouse fibroblasts (Fig. 4a10) but not detected in ZSD human fibroblasts (Fig. 4a12). ZSD mouse fibroblasts isolated from a similar mild ZSD mouse model were already shown to exhibit peroxisomal mosaicism (Berendse et al. 2019). Moreover, the PEX1-G844D protein expressed in ZSD mouse fibroblasts was shown to be expressed in normal quantity but with a lower functionality, meaning that

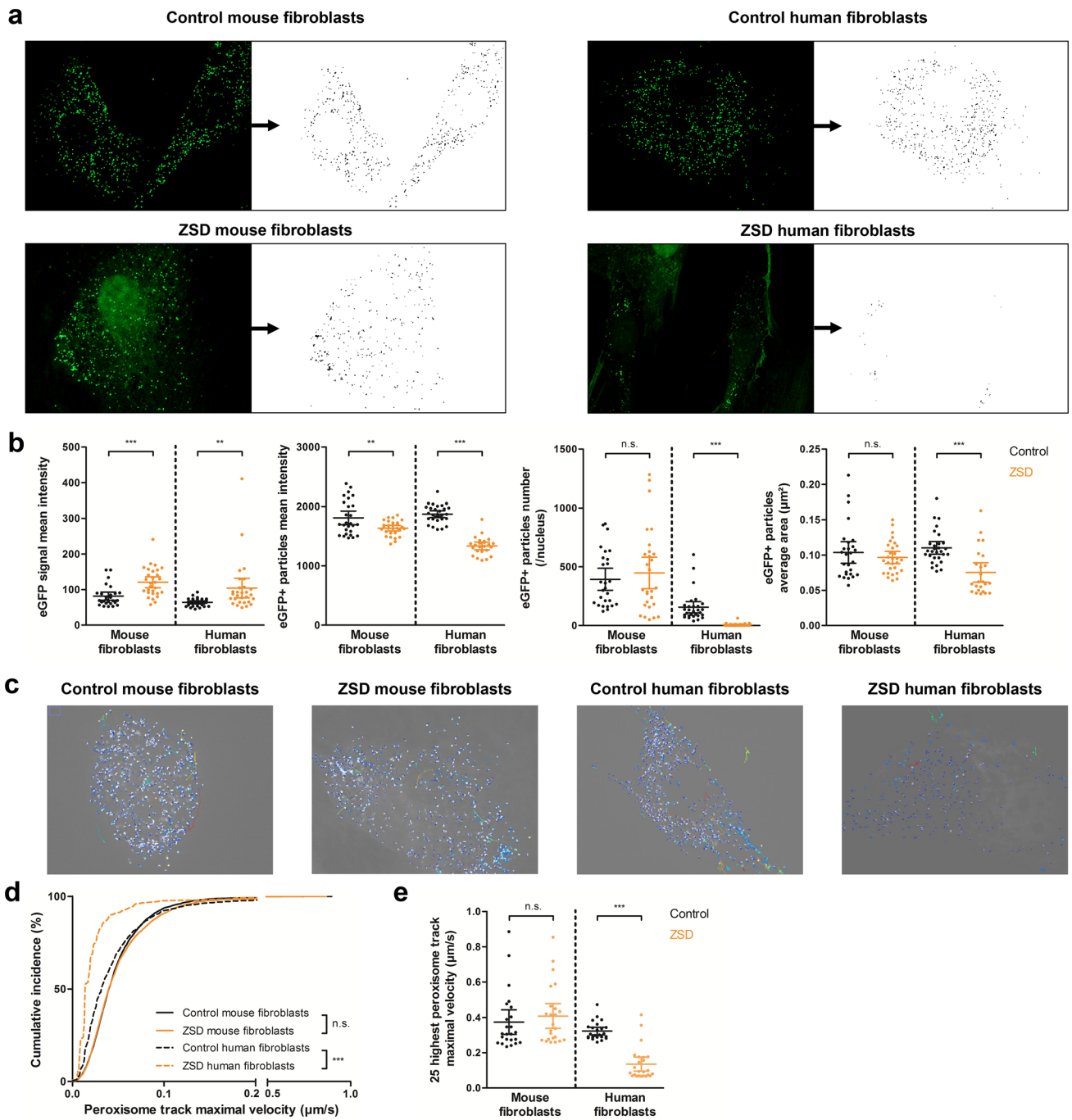

the mutation has a reduced impact on the protein (i.e., affecting only functionality but not stability) (Argyriou et al. 2019). In human fibroblasts, peroxisomal mosaicism was shown in cells from mildly affected ZSD patients (Giros et al. 1996; Mandel et al. 1994). In our study, ZSD human fibroblasts were collected from a ZSD patient presenting already in the neonatal period with facial dysmorphism, feeding disturbance, cholestasis, and typical biochemical abnormalities (Demaret et al. 2018). In conclusion, our method is able to detect PBD in cells from classical ZSD donors, but our tool is also sensitive enough to decipher PBD in cells with milder phenotype.

To our knowledge, this is the first report, validation, and public availability (Addgene #133282) of a lentiviral transfer plasmid encoding a peroxisome targeted marker. The strengths of this method are its security, stable protein expression evaluated in two eukaryote species, easy setup, and PB sensitivity similar to catalase staining. The use of a single transduction (compared to recurrent transfections required by Lipofectamine or microporation) and single

◂**Fig. 5** **a** Masks created by "AnalyzeParticles" tool from ImageJ software to detect and measure the enhanced green fluorescent protein (eGFP)-positive (eGFP+) particles in the four donors. **b** eGFP signal analysis from four cell donors transduced with eGFP–peroxisome targeting signal 1 (eGFP–PTS1) lentiviruses. eGFP signal mean intensity describes the eGFP average intensity value from the entire micrograph (left). eGFP+ particles mean intensity describes the eGFP average intensity value from the eGFP+ particles. eGFP signal mean intensity and eGFP+ particles mean intensity were, respectively, higher and lower in Zellweger spectrum disorder (ZSD) than in control fibroblasts. These results are explained by the fact that the eGFP–PTS1 remained diffuse in the cytosol of ZSD cells (higher eGFP signal mean intensity) because of the lack of peroxisomal import (lower eGFP+ particles mean intensity). eGFP+ particle number was normalized to nuclei for each picture. The eGFP+ particles average area describes the mean area of the eGFP+ particles (in μm^2). These last two parameters were significantly decreased in ZSD human fibroblasts. Unpaired Student's *t* test two-tailed, $n=30$, mean ± 95% confidence interval, n.s.: not significant, $^{**}p<0.01$, $^{***}p<0.001$. **c** eGFP + particles tracking performed by TrackMate plugin for ImageJ on eGFP–PTS1 transduced cells from four donors to measure peroxisome motility. White dots are eGFP+ particles (peroxisomes) and colored lines represent the track of each peroxisome along their displacement (blue to red lines reflect the slowest to the fastest particles). **d** Cumulative incidence of peroxisome track maximal velocity recorded for every eGFP+ particles in the four donors transduced with eGFP–PTS1. Unpaired Student's *t* test two-tailed, $n>400$, *n.s.* not significant, $^{***}p<0.001$. **e** 25 highest peroxisome track maximal velocity recorded in the four donors transduced with eGFP–PTS1. Unpaired Student's *t* test two-tailed, $n=25$, mean ± 95% confidence interval, *n.s.* not significant, $^{***}p<0.001$

signal (compared to catalase + PMP70 colocalization) make it suitable and convenient for high-throughput screening. Some limitations are inherent to the technology used like handling in a biosafety level 2 environment and cell sorting requirement to get 100% cell positivity. Yet, these steps are to be performed only once for a given cell type. In the future, eGFP–PTS1 transduced ZSD cell donors with different *PEX* mutations could be exposed to chaperones to evaluate their effect on the PBD (MacLean et al. 2019).

Conclusions

We developed an eGFP–PTS1 stable and highly potent third-generation lentiviral expression system in eukaryotic cells to study PB in vitro which allowed us to quantify and measure peroxisomes and their motility.

Acknowledgments We acknowledge the patients for their implication in the study, Caroline Bouzin for the help with immunofluorescent staining, Caroline Daems for her great cloning tips, Valery Payen for the useful discussions about lentivirus production, and Julie Vandewalle for the proofreading. pEGFP-C1 + SKL was a gift from Jay Brenman (Addgene plasmid #53450), pRRLSIN.cPPT.PGK-GFP.WPRE, pMDLg/pRRE, and pRSV-Rev were a gift from Didier Trono (Addgene plasmid #12252, #12251, and #12253), and pCMV-VSV-G was a gift from Bob Weinberg (Addgene plasmid #8454); we thank them for their contributions. We are thankful to the reviewers for their relevant remarks and suggestions.

Author contributions Conceptualization: TD, MN, and ES. Methodology: TD, GC, JR, and PVDS. Software: TD, GC, and PVDS. Validation: TD and JR. Formal analysis: TD. Data curation: TD. Writing—original draft preparation: TD. Writing—review and editing: TD, GC, JR, PVDS, MN, and ES. Supervision: MN and ES. Funding acquisition: TD and ES.

Funding Tanguy DEMARET is FRIA Grant Holder of the Fonds de la Recherche Scientifique-FNRS.

Compliance with ethical standards

Conflict of interest The authors declare no conflict of interest. The funders had no role in the design of the study; in the collection, analyses, or interpretation of data; in the writing of the manuscript, or in the decision to publish the results.

Ethical approval All procedures performed in studies involving human participants were in accordance with the ethical standards of the institutional research committee (Comission d'Ethique Hospitalo-Facultaire, Cliniques Universitaires Saint-Luc, F/2005/04) and with the 1964 Helsinki declaration and its later amendments or comparable ethical standards. All procedures performed in studies involving animals were in accordance with the ethical standards of the institution or practice at which the studies were conducted (Ethical Committee for Animal Experimentation at the Health Science Sector, UCLouvain, 2017/UCL/MD/006).

References

Argyriou C, D'Agostino MD, Braverman N (2016) Peroxisome biogenesis disorders. Transl Sci Rare Dis 1:111–144. https://doi.org/10.3233/trd-160003

Argyriou C, Polosa A, Cecyre B, Hsieh M, Di Pietro E, Cui W, Bouchard JF, Lachapelle P, Braverman N (2019) A longitudinal study of retinopathy in the PEX1-Gly844Asp mouse model for mild Zellweger Spectrum Disorder. Exp Eye Res. https://doi.org/10.1016/j.exer.2019.107713

Berendse K, Ebberink MS, Ijlst L, Poll-The BT, Wanders RJ, Waterham HR (2013) Arginine improves peroxisome functioning in cells from patients with a mild peroxisome biogenesis disorder. Orphanet J Rare Dis 8:138. https://doi.org/10.1186/1750-1172-8-138

Berendse K, Engelen M, Ferdinandusse S, Majoie CB, Waterham HR, Vaz FM, Koelman JH, Barth PG, Wanders RJ, Poll-The BT (2016) Zellweger spectrum disorders: clinical manifestations in patients surviving into adulthood. J Inherit Metab Dis 39:93–106. https://doi.org/10.1007/s10545-015-9880-2

Berendse K, Boek M, Gijbels M, Van der Wel NN, Klouwer FC, van den Bergh-Weerman MA, Shinde AB, Ofman R, Poll-The BT, Houten SM, Baes M, Wanders RJA, Waterham HR (2019) Liver disease predominates in a mouse model for mild human Zellweger spectrum disorder. Biochim Biophys Acta Mol Basis Dis. https://doi.org/10.1016/j.bbadis.2019.06.013

Brickner DG, Harada JJ, Olsen LJ (1997) Protein transport into higher plant peroxisomes. In vitro import assay provides evidence for

receptor involvement. Plant Physiol 113:1213–1221. https://doi.org/10.1104/pp.113.4.1213

Demaret T, Varma S, Stephenne X, Smets F, Scheers I, Wanders R, Van Maldergem L, Reding R, Sokal E (2018) Living-donor liver transplantation for mild Zellweger spectrum disorder: up to 17 years follow-up. Pediatr Transplant 22:e13112

Deosaran E, Larsen KB, Hua R, Sargent G, Wang Y, Kim S, Lamark T, Jauregui M, Law K, Lippincott-Schwartz J, Brech A, Johansen T, Kim PK (2013) NBR1 acts as an autophagy receptor for peroxisomes. J Cell Sci 126:939–952. https://doi.org/10.1242/jcs.114819

Dias AF, Francisco T, Rodrigues TA, Grou CP, Azevedo JE (2016) The first minutes in the life of a peroxisomal matrix protein. Biochem Biophys Acta 1863:814–820. https://doi.org/10.1016/j.bbamcr.2015.09.025

Ebberink MS, Mooijer PA, Gootjes J, Koster J, Wanders RJ, Waterham HR (2011) Genetic classification and mutational spectrum of more than 600 patients with a Zellweger syndrome spectrum disorder. Hum Mutat 32:59–69. https://doi.org/10.1002/humu.21388

Emmanouilidis L, Gopalswamy M, Passon DM, Wilmanns M, Sattler M (2016) Structural biology of the import pathways of peroxisomal matrix proteins. Biochem Biophys Acta 1863:804–813. https://doi.org/10.1016/j.bbamcr.2015.09.034

Farre JC, Mahalingam SS, Proietto M, Subramani S (2019) Peroxisome biogenesis, membrane contact sites, and quality control. EMBO Rep. https://doi.org/10.15252/embr.201846864

Fujiki Y (2016) Peroxisome biogenesis and human peroxisome-deficiency disorders. Proc Jpn Acad Ser B Phys Biol Sci 92:463–477. https://doi.org/10.2183/pjab.92.463

Giros M, Roels F, Prats J, Ruiz M, Ribes A, Espeel M, Wanders RJ, Schutgens RB, Pampols T (1996) Long survival in a case of peroxisomal biogenesis disorder with peroxisome mosaicism in the liver. Ann N Y Acad Sci 804:747–749. https://doi.org/10.1111/j.1749-6632.1996.tb18689.x

Hiebler S, Masuda T, Hacia JG, Moser AB, Faust PL, Liu A, Chowdhury N, Huang N, Lauer A, Bennett J, Watkins PA, Zack DJ, Braverman NE, Raymond GV, Steinberg SJ (2014) The Pex1-G844D mouse: a model for mild human Zellweger spectrum disorder. Mol Genet Metab 111:522–532. https://doi.org/10.1016/j.ymgme.2014.01.008

Hunter M, Yuan P, Vavilala D, Fox M (2019) Optimization of protein expression in mammalian cells. Curr Protoc Protein Sci 95:e77. https://doi.org/10.1002/cpps.77

Klouwer FC, Berendse K, Ferdinandusse S, Wanders RJ, Engelen M, Poll-The BT (2015) Zellweger spectrum disorders: clinical overview and management approach. Orphanet J Rare Dis 10:151. https://doi.org/10.1186/s13023-015-0368-9

Koster J, Waterham HR (2017) Transfection of primary human skin fibroblasts for peroxisomal studies. Methods Mol Biol (Clifton, NJ) 1595:63–67. https://doi.org/10.1007/978-1-4939-6937-1_7

Law KB, Bronte-Tinkew D, Di Pietro E, Snowden A, Jones RO, Moser A, Brumell JH, Braverman N, Kim PK (2017) The peroxisomal AAA ATPase complex prevents pexophagy and development of peroxisome biogenesis disorders. Autophagy 13:868–884. https://doi.org/10.1080/15548627.2017.1291470

MacLean GE, Argyriou C, Di Pietro E, Sun X, Birjandian S, Saberian P, Hacia JG, Braverman NE (2019) Zellweger spectrum disorder patient-derived fibroblasts with the PEX1-Gly843Asp allele recover peroxisome functions in response to flavonoids. J Cell Biochem 120:3243–3258. https://doi.org/10.1002/jcb.27591

Mandel H, Espeel M, Roels F, Sofer N, Luder A, Iancu TC, Aizin A, Berant M, Wanders RJ, Schutgens RB (1994) A new type of peroxisomal disorder with variable expression in liver and fibroblasts. J Pediatr 125:549–555. https://doi.org/10.1016/s0022-3476(94)70006-0

Marcassa E, Kallinos A, Jardine J, Rusilowicz-Jones EV, Martinez A, Kuehl S, Islinger M, Clague MJ, Urbe S (2018) Dual role of USP30 in controlling basal pexophagy and mitophagy. EMBO Rep. https://doi.org/10.15252/embr.201745595

Mast FD, Jamakhandi A, Saleem RA, Dilworth DJ, Rogers RS, Rachubinski RA, Aitchison JD (2016) Peroxins Pex30 and Pex29 dynamically associate with reticulons to regulate peroxisome biogenesis from the endoplasmic reticulum. J Biol Chem 291:15408–15427. https://doi.org/10.1074/jbc.m116.728154

Matsunami M, Shimozawa N, Fukuda A, Kumagai T, Kubota M, Chong PF, Kasahara M (2016) Living-donor liver transplantation from a heterozygous parent for infantile refsum disease. Pediatrics. https://doi.org/10.1542/peds.2015-3102

Metz J, Castro IG, Schrader M (2017) Peroxisome motility measurement and quantification assay. Bio-protocol. https://doi.org/10.21769/bioprotoc.2536

Neuhaus A, Eggeling C, Erdmann R, Schliebs W (2016) Why do peroxisomes associate with the cytoskeleton? Biochem Biophys Acta 1863:1019–1026. https://doi.org/10.1016/j.bbamcr.2015.11.022

Santos MJ, Imanaka T, Shio H, Small GM, Lazarow PB (1988) Peroxisomal membrane ghosts in Zellweger syndrome—aberrant organelle assembly. Science 239:1536–1538. https://doi.org/10.1126/science.3281254

Schrader TA, Islinger M, Schrader M (2017) Detection and immunolabeling of peroxisomal proteins. Methods Mol Biol (Clifton, NJ) 1595:113–130. https://doi.org/10.1007/978-1-4939-6937-1_12

Sexton JZ, He Q, Forsberg LJ, Brenman JE (2010) High content screening for non-classical peroxisome proliferators. Int J High Throughput Screen 2010:127–140. https://doi.org/10.2147/ijhts.s10547

Sokal EM, Smets F, Bourgois A, Van Maldergem L, Buts JP, Reding R, Bernard Otte J, Evrard V, Latinne D, Vincent MF, Moser A, Soriano HE (2003) Hepatocyte transplantation in a 4-year-old girl with peroxisomal biogenesis disease: technique, safety, and metabolic follow-up. Transplantation 76:735–738. https://doi.org/10.1097/01.tp.0000077420.81365.53

Soliman K, Gottfert F, Rosewich H, Thoms S, Gartner J (2018) Super-resolution imaging reveals the sub-diffraction phenotype of Zellweger Syndrome ghosts and wild-type peroxisomes. Sci Rep 8:7809. https://doi.org/10.1038/s41598-018-24119-2

Tinevez JY, Perry N, Schindelin J, Hoopes GM, Reynolds GD, Laplantine E, Bednarek SY, Shorte SL, Eliceiri KW (2017) TrackMate: an open and extensible platform for single-particle tracking. Methods (San Diego, Calif) 115:80–90. https://doi.org/10.1016/j.ymeth.2016.09.016

Tymms MJ, Kola I (2001) Gene knockout protocols. Methods in molecular biology, vol 158. Humana Press Inc., Totowa

Van Maldergem L, Moser AB, Vincent MF, Roland D, Reding R, Otte JB, Wanders RJ, Sokal E (2005) Orthotopic liver transplantation from a living-related donor in an infant with a peroxisome biogenesis defect of the infantile Refsum disease type. J Inherit Metab Dis 28:593–600. https://doi.org/10.1007/s10545-005-0593-9

Wanders RJ (2014) Metabolic functions of peroxisomes in health and disease. Biochimie 98:36–44. https://doi.org/10.1016/j.biochi.2013.08.022

Wei H, Kemp S, McGuinness MC, Moser AB, Smith KD (2000) Pharmacological induction of peroxisomes in peroxisome biogenesis disorders. Ann Neurol 47:286–296

Zhang R, Chen L, Jiralerspong S, Snowden A, Steinberg S, Braverman N (2010) Recovery of PEX1-Gly843Asp peroxisome dysfunction by small-molecule compounds. Proc Natl Acad Sci U S A 107:5569–5574. https://doi.org/10.1073/pnas.0914960107

Publisher's Note Springer Nature remains neutral with regard to jurisdictional claims in published maps and institutional affiliations.